Korean J. Chem. Eng., 40(4), 802-809 (2023)
DOI: 10.1007/s11814-023-1392-4

pISSN: 0256-1115
eISSN: 1975-7220

Cyanoethyl-guar gum as an effective polymer binder for lithium titanate electrode of the lithium-ion battery

Inyeong Choi‡, Bolormaa Gendensuren‡, Jieun Lee, and Eun-Suok Oh†

School of Chemical Engineering, University of Ulsan, 93 Daehakro, Nam-gu, Ulsan 44610, Korea
(*Received 21 July 2022 • Revised 31 October 2022 • Accepted 29 December 2022*)

Abstract−Unlike high-capacity silicon active materials, lithium titanate $Li_4Ti_5O_{12}$ (LTO) as an anode material in lithium-ion battery shows almost no volume change during the charge/discharge processes. This fact rather neglects the importance of binder materials for the LTO electrode. A few research efforts indicate that a polymer binder aiding rapid ion or electron transfer is suitable for the LTO electrode. In this study, the synergetic effect between branched guar gum polysaccharide and polar nitrile groups was thoroughly investigated as a promising binder candidate for the LTO electrode. The cyanoethyl-guar gum binder synthesized by a straightforward cyanoethylation of guar gum with acrylonitrile leads to lower resistance on lithium-ion transport and electrolyte penetration due to the strongly polar nitrile groups. Compared to the pristine guar gum binder-based LTO electrode, therefore, the LTO electrode containing the cyanoethyl-guar gum binder exhibits superior rate performance with improved kinetics.

Keywords: Water-soluble Binder, Guar Gum, Cyanoethyl Group, LTO Electrode

INTRODUCTION

Graphite as an anodic material of the lithium-ion battery (LIB) has been successfully used, due to its moderate energy and power density. Meanwhile, its application to electric vehicles (EV) and energy storage systems (ESS) that require higher power and energy density with longer cycle life is limited. In this respect, lithium titanium oxide ($Li_4Ti_5O_{12}$, LTO) shows good cyclability and rapid lithium ion transport because of its extremely stable spinel structure, so that it can be suitable for the anode material of LIBs used in the EV and ESS [1-3], though its gravimetric energy density is less than that of graphite. Much research has sought ways to improve the electrochemical properties of LTO, but little attention has been paid to the development of a suitable binder for LTO materials.

Most of the recent studies on binders have focused on developing a new kind of polymer that is appropriate for high-capacity silicon anodes [4-7]. Since during the charge/discharge process, the high-capacity anodes experience severe volume changes, the adhesion capability of polymer binder is relatively more important than the other properties of binder, such as ion or electron transport. In this sense, linear stiff polymers containing hydroxyl or carboxyl functional groups are favorable to high-capacity anodes [8-11]. These groups form strong hydrogen bonds in the electrode, leading to resistance to organic carbonate electrolyte, and thus maintaining strong adhesion during use. Unlike silicon, LTO materials show almost zero strain during the insertion/desertion processes with lithium ions. This fact makes a difference in finding an appropriate polymer binder for the LTO anodes, compared to the silicon anodes. A few research efforts on polymer binder for LTO have been carried out [12-14] and reviewed in detail in our previous works [15-18]. It was concluded that polymer aiding rapid ion or electron transfer could be more suitable for LTO, so long as it achieved critical adhesion in LTO electrodes.

From our previous results [16], guar gum (GG) binders, branched polysaccharides, facilitated the transport of lithium ions in LTO electrodes when compared to carboxymethyl cellulose (CMC) binder, linear polysaccharide, even though their adhesive strength was not as strong as that of CMC. This is attributed to the large extent of electrolyte uptake and the large LTO surface exposed to electrolyte when gum binders are used. Moreover, polymer binders containing numerous nitrile groups (C≡N), such as polyacrylonitrile (PAN) and poly(acrylonitrile-butylacrylate), showed good binder properties, because nitrile groups have strong polarity caused by very electronegative nitrogen [19-21]. Nitrile groups can also form interactions with their environment by hydrogen bonding and dipole-dipole interactions. In this study, therefore, the synergetic effect between branched guar gum polysaccharide and the nitrile groups was thoroughly investigated as a promising binder candidate for LTO electrode. Cyanoethylation of GG to introduce nitrile groups to GG was achieved through the reaction between GG and acrylonitrile in the presence of the catalytic action of sodium hydroxide [22-24]. As-synthesized cyanoethyl-guar gum (CGG), containing nitrile groups, was compared to original guar gum binders through a variety of electrochemical characterization tools.

EXPERIMENT

1. Synthesis of Cyanoethyl-Guar Gum

Guar gum was cyanoethylated under a basic atmosphere. Four (4) g of guar gum powder (Sigma-Aldrich) was homogeneously dissolved in 120 mL water, and 1 g of 50% sodium hydroxide solution

†To whom correspondence should be addressed.
E-mail: esoh1@ulsan.ac.kr
‡Equally contributed to this work.

was then added while being mechanically stirred. Subsequently, 1 g of acrylonitrile was slowly dropped into a flask reactor, maintaining the temperature at approximately 50 °C for 0.5 h. Here the molar ratio between acrylonitrile (AN) and GG was 1 : 2.5. The reaction was continued with nitrogen purging for 3 h. Finally, the resultant solution was washed in alcohol, collected by filtration, and then dried in vacuum oven at 60 °C. After drying, the power was dissolved in a proper amount of water, to be used for LTO electrodes.

2. Fabrication of LTO Electrodes and Cells

To make the LTO electrode slurry, 85 wt% LTO (d_{avg}=10 μm, Posco ESM Co.) as the active material, 5 wt% GG or CGG binder, and 10 wt% super-P (SP) as the conducting agent were mixed in a planetary ball mill (Pulverisette 7, Fritsch; speed 320 rpm) with a proper amount of water for 1 h. The slurry was coated onto a 20 μm thick copper foil, and dried in convection oven at 60 °C for 30 min, followed by vacuum drying overnight at 70 °C. Two mass loadings of the LTO electrodes, (4.0±0.1) mg cm^{-2} and (6.4±0.1) mg cm^{-2} were adopted. In addition, two other electrode compositions, LTO : SP : CGG=87 : 10 : 3 and 90 : 5 : 5, were also chosen to investigate more thoroughly the effect of cyanoethylation. These loadings and compositions are close to those in previous studies in Table S1 of the supporting information. CR2016 coin-type half-cells were manufactured in an argon-filled glove box. The LTO electrode was assembled with lithium metal as a counter electrode, and electrolyte solution (Panaxetec Co.) of 1 M $LiPF_6$ in ethylene carbonate (EC), ethylmethyl carbonate (EMC), and dimethyl carbonate (DMC) with 1 : 1 : 1 volumetric ratio.

3. Physical Characterization

The interaction between guar gum and acrylonitrile was analyzed using Fourier-transform infrared spectroscopy (FT-IR, Thermo Scientific, Nicolet IR 200), operating in the range (4,000-400) cm^{-1}. X-ray photoelectron spectroscopy (XPS, ESCALAB 250, Thermo Fisher Scientific) was performed to analyze the surface of the LTO electrodes. The electrical resistance of the LTO electrode sheet was measured using a 46-multipoint probe system (RM2610, HIOKI E.E. Co.). The adhesion strength of the electrodes was measured by 180° peeling of 20 mm width electrode strips with a peel rate of 50 mm min^{-1}, using a texture analyzer (TA-PLUS, Lloyd Instruments Ltd.). The binder film was immersed into solute-free electrolyte solution, EC : EMC : DMC=1 : 1 : 1 (vol.) for two days to measure the amount of electrolyte uptake. To estimate the electrolyte wettability of binder, the contact angles of thin binder films were measured as a function of time exposed to an electrolyte droplet using a video-connected device (Theta Lite 100, KSV Instrument Ltd., Finland).

To obtain ionic conductivity of the binder film, an impedance analysis of two stainless-steel (SS) electrodes with SS|binder film|SS configuration was conducted at a frequency range from 0.01 Hz to 10^6 Hz with the AC amplitude of 10 mV. With the bulk resistance of the binder film determined from the high frequency intercept of the impedance spectrum, the ionic conductivity (σ) was calculated using $\sigma=d/(A\times R_b)$ where d is the thickness of the binder film (110±5 μm) and A is area of the SS electrodes (0.78 cm^2).

4. Electrochemical Characterization

The electrochemical performance of the coin cells was measured by galvanostatic charge/discharge in the potential range (1-2.6) V, using a battery test system (PNE solution Co., Korea) with a constant current mode of 0.1 C rate for the first two cycles, and 1 C rate for the next 100 cycles. The rate capability of the LTO electrodes was also tested at various charge/discharge current rates, up to 20 C. The electrochemical impedance measurements were carried out by potentiostat (VSP, BioLogic Science Instruments) at a frequency range of (0.01 Hz to 100 kHz). To investigate the electrochemical reactions of the electrodes, cyclic voltammetry (CV) was also performed at various scan rates of (0.5 to 20) mV s^{-1} in the range (1-2.6) V using the device.

RESULTS AND DISCUSSION

CGG was synthesized with the simple addition of AN to GG in a basic solution, as shown in Fig. 1(a). FT-IR characterization was performed to confirm the chemical bonding between acrylonitrile and GG, and the results are shown in Fig. 1(b). The FT-IR spectrum of GG reveals the strong stretching band of -OH at 3,306 cm^{-1}, the narrow peak of $-CH_2$ at 2,919 cm^{-1}, and the bending band of $-CH_2$ at 1,372 cm^{-1}. The absorption band of -OH groups and the bending of C-O-C also appear at (1,646 and 1,013) cm^{-1}, respec-

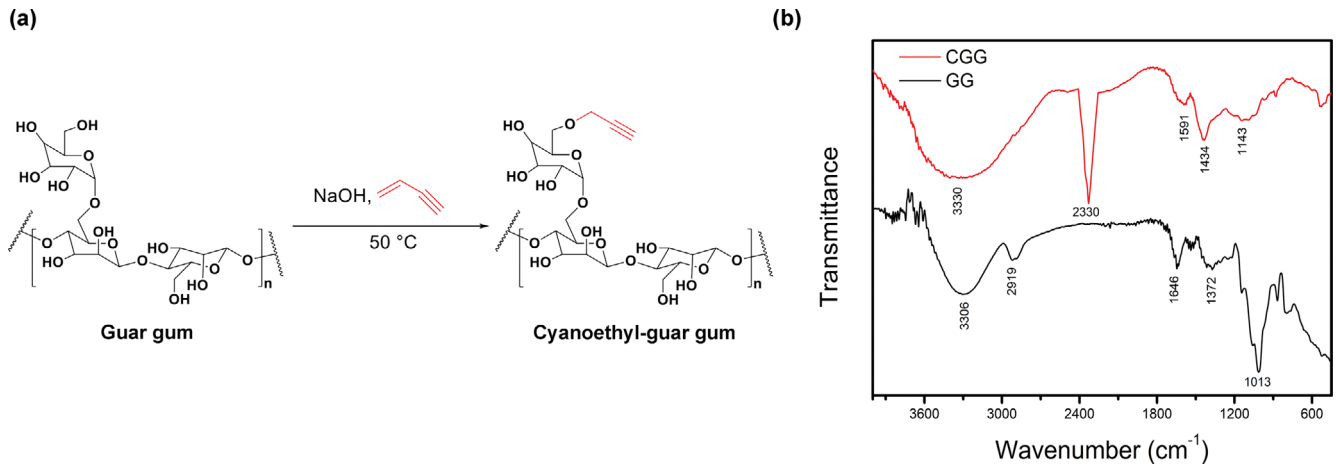

Fig. 1. (a) Synthesis of cyanoethyl-guar gum, and (b) FT-IR spectra of guar gum and cyanoethyl-guar gum.

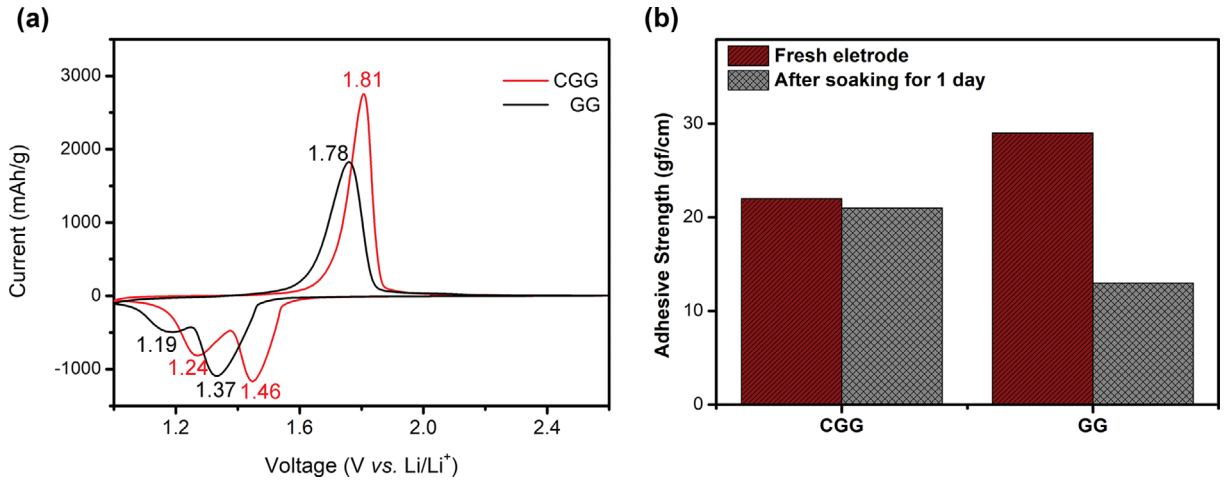

Fig. 2. (a) Cyclic voltammograms of the LTO electrodes containing GG and CGG binders. (b) Adhesion strength of the LTO electrodes before and after soaking in electrolyte for 24 h.

tively. In contrast, the peaks related to -OH functional groups become weaker in the FT-IR spectrum of CGG, and appear at (3,330 and 1,591) cm^{-1}, because some of the groups participate in the reaction to form nitrile groups (-C≡N) with AN [25,26]. The sharp peaks attributed to the nitrile group newly appear at ~2,330 cm^{-1} [27,28], indicating the successful synthesis of CGG by the simple cyanoethylation reaction.

In the process of developing a new binder material or modifying an existing binder material, two prerequisite tests should be done before applying it to the binder of an electrode: electrochemical stability, and adhesion capability. These qualities are indispensable to maintain the binding character of the binder, and to maintain the good electrical network of the electrode during its use. First, the electrochemical stability of the binder was indirectly examined through the CV of the LTO electrodes containing GG or CGG binder, and Fig. 2(a) shows the result. They both have a typical redox pair of peaks between (1.37 and 1.81) V, attributed to the Li intercalation/deintercalation to LTO, and a cathodic peak around 1.2 V [29,30]. The cathodic peak might be assigned to the reduction that originates from the Li^+ doping to polymer materials. A similar peak was observed from the LTO/Polyaniline electrode, and the LTO electrode containing poly(vinylidene fluoride-co-hexafluoropropylene) binder [31,32]. These typical CV profiles with no peculiar peaks originating from the binder imply that both GG and CGG are electrochemically stable in the working voltage of the LTO electrode. On the other hand, the potential difference of redox peaks, $\Delta E_p = |E_p^{anodic} - E_p^{cathodic}|$, of the LTO/GG electrode is 0.41 V with lower peak currents, whereas the value of ΔE_p for the LTO/CGG electrode is 0.35 V, with higher peaks. This narrow voltage gap and intensive current peak of the LTO/CGG electrode indicates that the LTO electrode manufactured with the CGG binder has lower polarization resistance and is more electrochemically active than that composed of the GG binder.

Second, the essential property of a polymer binder is the ability to adhere all electrode components to the current collector and themselves, to maintain an electrically conductive electrode layer. This is generally estimated via a 180° peel strength test of the electrode. As shown in Fig. 2(b), the fresh LTO electrode containing CGG binder shows weaker adhesion strength than that containing the pristine GG. This result is expected from the chemical structure written in Fig. 1(a). The introduction of nitrile groups to GG replaces some of the hydroxyl groups in GG, which forms strong hydrogen bonds with active materials as well as the current collector, even though the polar nitrile groups also form certain interactions with the environment by hydrogen bonding and dipole-dipole interactions [20,26]. However, after soaking the electrode in excess electrolyte solution for 24 h, the interaction of GG is seriously weakened, compared to CGG, even though the amounts of electrolyte uptake of the GG and CGG binders for two days are nearly equal as much as 25% as shown in Table S2. In general, the electrolyte penetration to binder weakens the interaction of binder, leading to the decrease in its adhesion capability. The introduction of nitrile groups diminishes the risk of severe adhesion decrease originating from the electrolyte penetration of GG, and thus helps to maintain the electrical network during the use.

These advantages of the CGG binder for the LTO electrode lead to subsequent electrochemical performance tests in comparison with the GG binder. Fig. 3 shows these results. The initial discharge capacities of the LTO electrodes containing CGG or the pristine GG binder are (184.3 and 176.1) mAh g^{-1} measured at 0.1 C current, respectively. The LTO/CGG shows a reversible discharge capacity of ~148.0 mAh g^{-1} for 100 cycles at 1 C current, whereas the LTO/GG exhibits 142.8 mAh g^{-1} discharge capacity after 100 cycles. Even though when 1 C current rate is employed, the difference in the discharge capacity and the Coulombic efficiency is not large in the whole charge/discharge cycle, as the current rate increases from (1 to 20) C, the difference gradually increases, as shown in Fig. 3(b). Compared to the LTO/GG electrode, the LTO/CGG electrode exhibits much better cyclic performance at such high current rates of more than 5 C. For example, the LTO/CGG electrode retains the average specific capacity of 55.1 mAh g^{-1} at 20 C, which is 36.8% of the capacity at 1 C. In contrast, the LTO/GG electrode has 32.0 mAh g^{-1} and 22.6%, respectively, at the 20 C current rate. Nevertheless, both LTO electrodes fully restore their capacities when they are

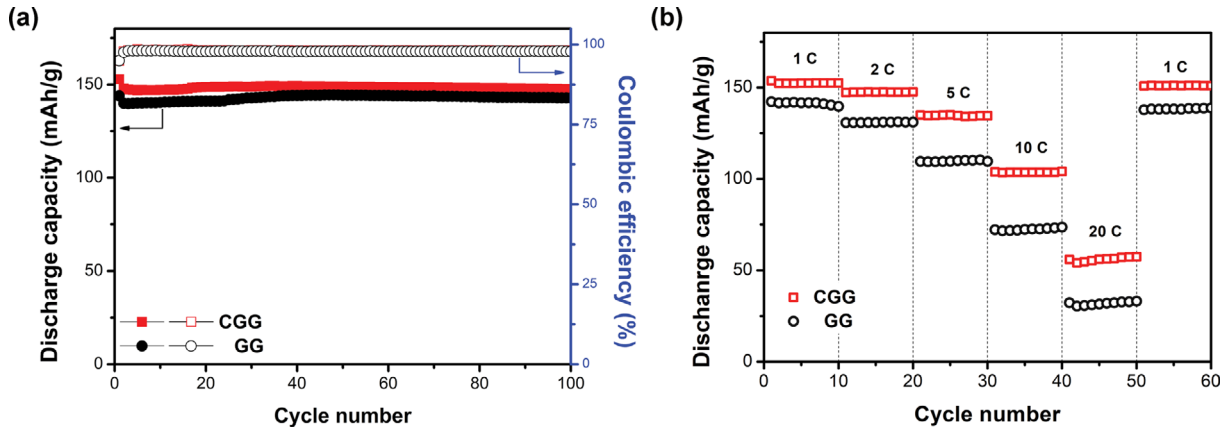

Fig. 3. Electrochemical performance of the LTO electrodes, (a) cycling performance, and (b) rate-capability test.

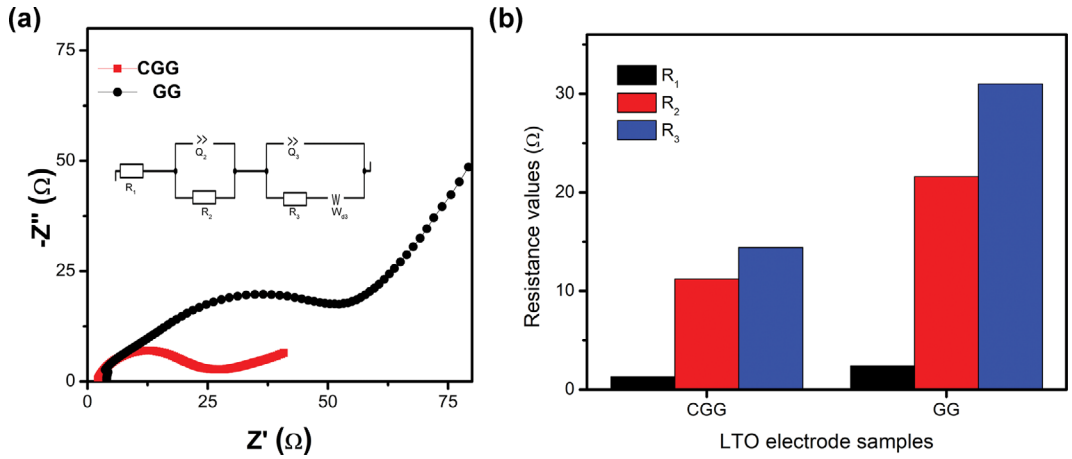

Fig. 4. Impedance of the LTO electrodes containing GG or CGG binder: (a) Nyquist plot, and (b) resistances.

back to moderate 1 C cycles from 20 C high rates. Therefore, no severe impact occurs in the electrodes, even at such high current rates.

To analyze the positive effect by the CGG binder in more detail, a few characteristic techniques were performed, and their results are shown below. Above all, EIS spectra of the LTO electrodes should be discussed to compare their impedances for the electrochemical reactions. Fig. 4(a) illustrates the Nyquist plots of the electrodes obtained after two cycles at 1 C, and they are fitted using an equivalent circuit, $R_1+Q_2|R_2+Q_3|(R_3+W_d)$, drawn inside to obtain the resistances. Herein, the electrolyte ionic resistance (R_1) corresponds to the intercept extrapolated to extremely high frequency, i.e., to the real axis, and the resistance (R_2) from high- to middle-frequency range is characterized by Li-ion transport across solid electrolyte interface (SEI) [19,33]. The charge transport resistance (R_3) measured using the size of the semicircle at middle- to low-frequency range is caused by the electrochemical reaction at the electrode-electrolyte interface layer [33,34]. In addition, R_3 is also affected by both the transformation of Li^+ ions to Li by accepting an electron in the electrode, and the electronic conductivity of electrode [34,35]. Fig. 4(b) shows the values of the resistances. The LTO electrode containing GG binder has (21.6 and 31.0) Ω as R_2 and R_3, respectively, whereas the LTO electrode containing CGG binder shows much smaller resistances, of R_2=11.2 Ω and R_3=14.4 Ω. Therefore, the decrease in the resistances on the electrochemical reactions by the cyanoethylation of GG binder must contribute to the improvement of the electrochemical performance of the LTO electrodes, as shown in Fig. 3.

The lithium-ion transport was qualitatively and quantitatively examined through the contact angle of binder films and the CV of the LTO electrodes at various scan rates. Fig. 5(a) indicates that the cyanoethylation of GG improves the affinity of GG to carbonate electrolyte, contributing to lithium-ion transport. This is consistent with our previous result that polyacrylonitrile composed of cyano functional groups had the lowest contact angle, when compared to CMC and polyvinylidene fluoride, due to the high affinity between polar nitrile groups and carbonates [20]. Furthermore, the CV profiles measured at the different scan rate from (0.1 to 20) mV s^{-1} in Figs. 5(b) & (c) provide some information on lithium-ion transport in the LTO electrode. Expected from the result in Fig. 2(a), the redox peaks of the LTO/CGG are stronger and wider current at any scan rates than those of the LTO/GG electrode, because the LTO/CGG is electrochemically more active than the LTO/GG.

The Randles-Ševčík equation [36-38] describes the dependence

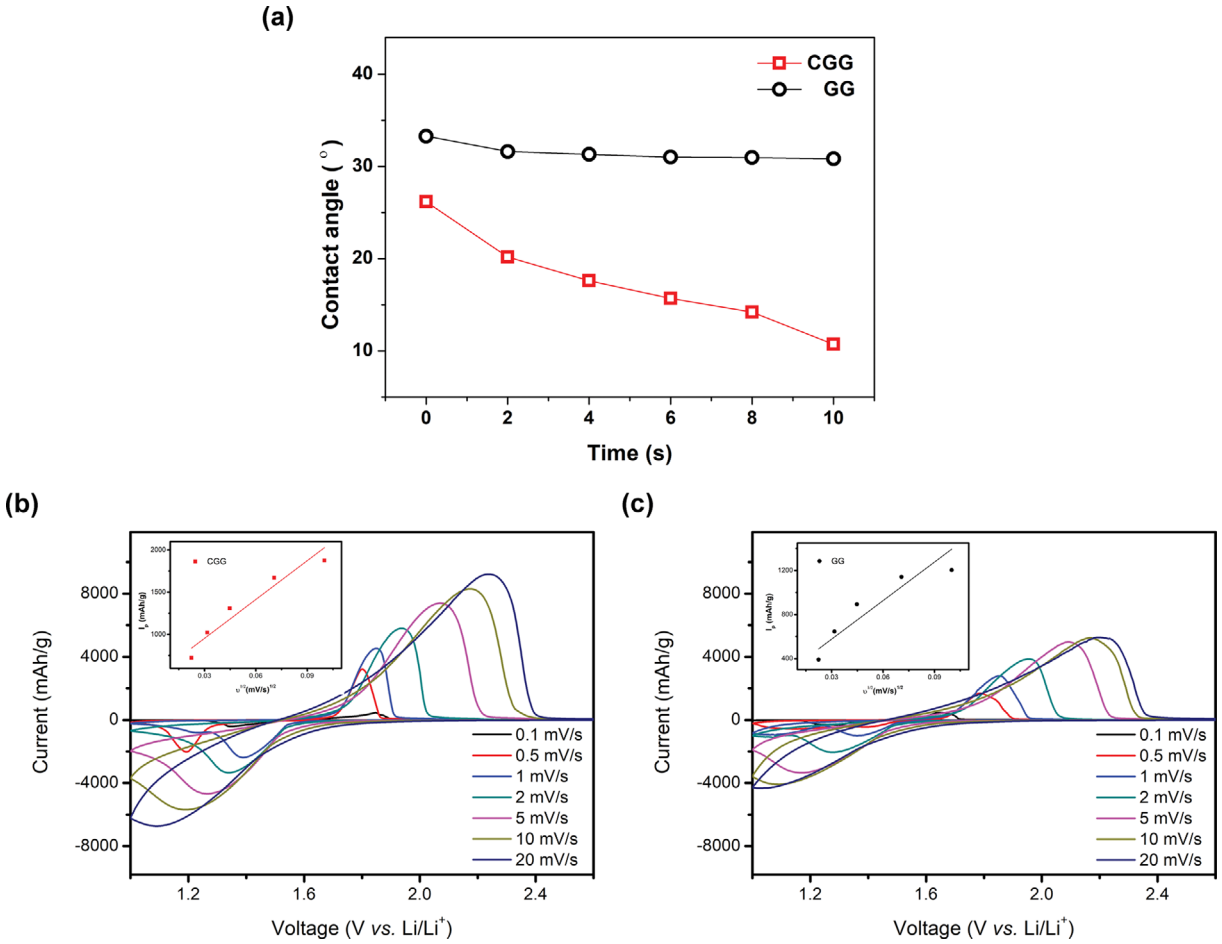

Fig. 5. (a) Contact angles of the binder film: GG and CGG, and (b) and (c) the CVs of the LTO electrodes containing CGG and GG at each scan rate, respectively.

of the peak currents on the scan rate to calculate the diffusion coefficient of lithium ions in an electrode, as follows:

$$I_p = 2.69\times10^5 An^{3/2}C_0D^{1/2}v^{1/2}$$

where, I_p is the peak current, n is the total number of the electrons transferred, A is the electrode surface area, C_0 is the concentration of reactants, D is the diffusion coefficient of lithium ion in an electrode, and v is the scan rate. From the slopes between I_p and $v^{1/2}$ shown inside the figure, the Li^+ diffusion coefficients of lithium-ion are 3.19×10^{-8} cm^2 s^{-1} for the LTO/CGG, and 1.03×10^{-8} cm^2 s^{-1} for the LTO/GG electrode, respectively. This result is also consistent with the previous studies that cyanoethyl-based polymers exhibit high ion conductivity and Li^+ transfer number in electrolyte of LIB, due to the interaction between nitrile groups (-C≡N) and Li^+ in carbonate electrolyte by the intrinsic lone pair in the nitrile groups [39-41]. Therefore, the improved lithium-ion transport contributes to the lower transfer resistances in Fig. 4 by the cyanoethylation of GG. In summary of Figs. 4 & 5, the CGG binder leads to better lithium-ion intercalation/deintercalation kinetics in the LTO electrode.

Depending on the interaction between polymeric binder and active materials, the binder covers the surface of active materials differently. Inhomogeneous and broad surface binder coverage is unfavorable for lithium ion transport, because the ionic conductivity of the polymer is significantly lower than that of the electrolyte [16,20,42]. Kovalenko et al. [11] reported that the ionic conductivity of alginate binder, whose structure is very similar to guar gum, was approximately ~10^{-8} S cm^{-1}, whereas liquid electrolyte normally has an ionic conductivity of ~10^{-3} S cm^{-1}. In a very similar way, the ionic conductivities of the electrolyte-soaked binder films were measured using an impedance spectroscopy and are listed in Table S2. Though the introduction of nitrile groups improves the ionic conductivity of GG from 1.87×10^{-7} S cm^{-1} to 2.59×10^{-7} S cm^{-1}, it is still much lower than liquid electrolyte. In this respect, it is desirable for the binder to cover the active materials in a narrow and homogeneous area. The XPS analysis of the LTO electrodes provides insight into the surface coverage by the binder [43], and Fig. 6 shows its result. Compared to the LTO/GG electrode, the LTO/CGG electrode exhibits a decrease in the C 1s peak at 282.64 eV, which originates from the carbon in guar gum. In contrast, the LTO/CGG electrode shows stronger peak intensity of Ti 2p, which is assigned to Ti^{4+} oxidation state, rather than the LTO/GG electrode. These imply that when the cyanoethylated GG is used as the binder for the LTO electrode, the broader portion of the surface in the LTO active materials is not covered by adhesive polymer binder and is directly exposed to liquid electrolyte. This can explain why

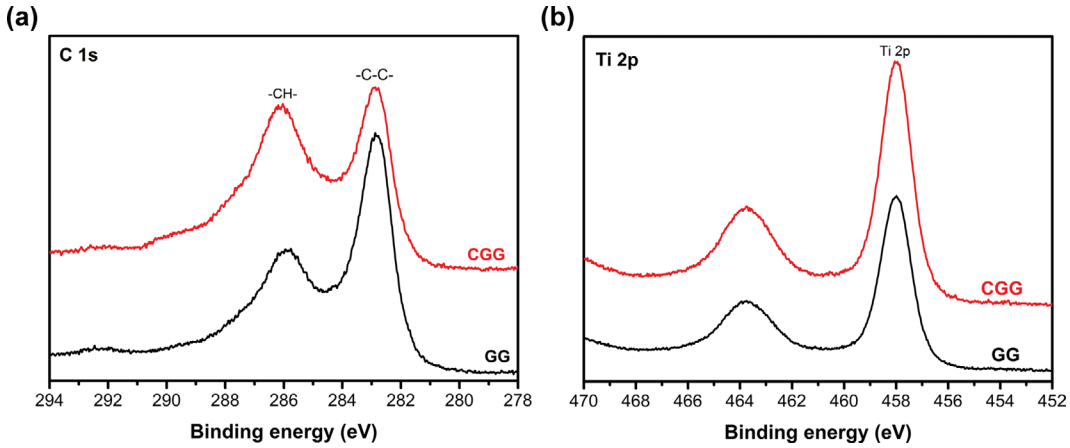

Fig. 6. XPS (a) C 1s and (b) Ti 2p peaks of the LTO electrodes containing CGG or GG binder.

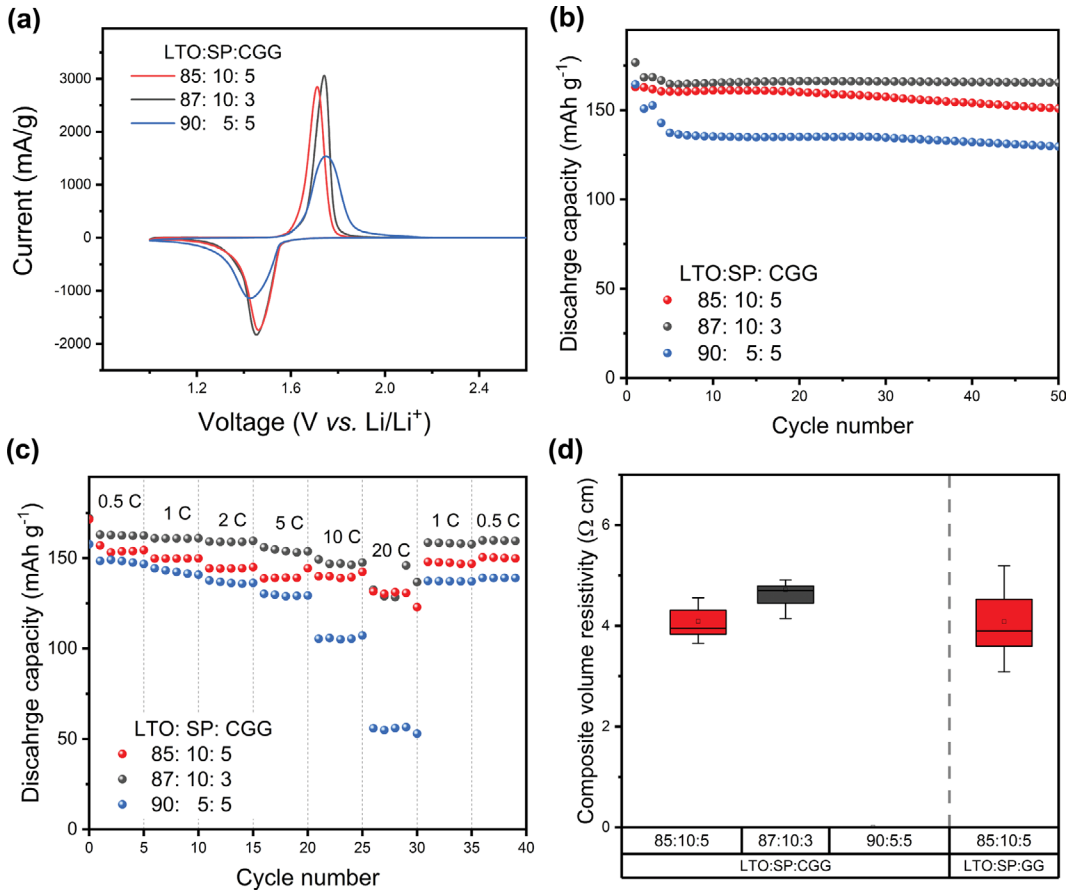

Fig. 7. Electrochemical performance of the LTO/CGG electrodes composed of three different electrode compositions: (a) CV profiles, (b) cycling performance, (c) c-rate capability test, and (d) composite volume resistivity. Here the mass loading of the electrodes is 6.4±0.1 mg cm^{-2}.

the adhesion is reduced when the nitrile group (-CN) is introduced to the GG, as shown in Fig. 2(b). In addition, the narrow surface coverage by the CGG binder helps to effectively improve the lithium-ion transport, as illustrated in Figs. 4 & 5. The increase in the amount of exposed titanium must contribute to the better electrochemical performance, as evident in the different C rates in Fig. 3(b).

The mass loading of the LTO electrodes was increased from (4.0±0.1) to (6.4±0.1) mg cm^{-2} and the effect of cyanoethylation of binder on their performance was also investigated. As seen in Fig. S1, the initial and cycled capacities of the LTO/CGG electrode are higher than the LTO/GG electrode with more stable cyclic reten-

tion and less polarization resistance. In addition, the change in the electrode thickness after 150 cycles slightly decreases from 2.61% to 2.15% when the GG binder is switched to the CGG binder. This can be attributed to better adhesion stability of CGG even after electrolyte soaking, as shown in Fig. 2(b). With the high mass loading of (6.4±0.1) mg cm^{-2}, two more LTO electrodes composed of LTO : SP : Binder=87 : 10 : 3 and 90 : 5 : 5 were manufactured to improve the performance of the CGG-based LTO electrodes. The results are in Fig. 7. Compared to the LTO electrodes composed of 10% SP, the 5% SP-containing LTO electrode shows lower redox peaks and broader peak difference in its CV profile, leading to worse electrochemical performance on its cycle and rate-capability tests (Fig. 7(b), (c)). Because the LTO material is not a good conductor of electricity, a relatively small amount of SP conductive agent in the LTO electrode seriously degrades the electrochemical performance of the electrode. This is proven in the composite volume resistivity of Fig. 7(d) and the interface resistance of Fig. S2 of the supporting information. The 10% SP samples show similar resistivity and resistance, whereas those of the 5% SP sample, the 90 : 5 : 5 LTO electrode, are over the device range. In contrast, the decrease in the binder content of the LTO electrode from 5 wt% to 3 wt% is favorable for its electrochemical performance as displayed in Fig. 7(b), (c), as expected because the polymer binder is naturally an electrical insulator. However, care should be taken in choosing an appropriate amount of binder because it greatly affects electrode manufacturing process including adhesion.

CONCLUSION

We successfully synthesized cyanoethylated guar gum (CGG) by a straightforward cyanoethylation reaction of GG with acrylonitrile in aqueous NaOH solution. The CGG binder for the LTO electrode leads to favorable environments for the electrochemical kinetics of the LTO active materials by lower resistances on lithium-ion transport and electrolyte penetration. This is due to the high affinity of polar nitrile groups with carbonates, and the existence of a lone pair in the nitrile group, leading to lithium positive ions. In addition, the cyanoethylated CGG binder leads to a narrow and homogeneous surface coverage of the binder on the surface of active material, indicating broader LTO surface directly exposed to electrolyte. This also contributes to better lithium-ion transport in the LTO electrode, though the electrode adhesion is slightly diminished. Therefore, it is remarked that when compared to the LTO/GG electrode, the LTO/CGG electrode has lower polarization potential and much lower charge-transfer resistance. Finally, the electrochemical performance of the LTO electrode containing cyanoethylated GG binder is superior to that of the LTO containing the pristine GG. For example, the LTO/CGG retains 36.8% capacity at 20 C in comparison with 1 C, whereas the LTO/GG has only 22.6%. Consequently, the cyanoethylation of GG binder is an efficient way to enhance the electrochemical performance of LTO active materials.

ACKNOWLEDGEMENTS

The study was supported by the 2021 research fund of the University of Ulsan.

SUPPORTING INFORMATION

Additional information as noted in the text. This information is available via the Internet at http://www.springer.com/chemistry/journal/11814.

REFERENCES

1. S. Chauque, F. Y. Oliva, A. Visintin, D. Barraco, E. P. M. Leiva and O. R. Cámara, *J. Electroanal. Chem.*, **799**, 142 (2017).
2. H. Yan, D. Zhang, Qilu, X. Duo and X. Sheng, *Ceram. Int.*, **47**, 5870 (2021).
3. C. Wu, Y. Wang, G. Ma and X. Zheng, *Electrochem. Commun.*, **131**, 107119 (2021).
4. M. Murase, N. Yabuuchi, Z.-J. Han, J.-Y. Son, Y.-T. Cui, H. Oji and S. Komaba, *ChemSusChem.*, **5**, 2307 (2021).
5. N.-S. Choi, S.-Y. Ha, Y. Lee, J. Y. Jang, M.-H. Jeong, W. C. Shin and M. Ue, *J. Electrochem. Sci. Technol.*, **6**, 35 (2015).
6. P.-F. Cao, G. Yang, B. Li, Y. Zhang, S. Zhao, S. Zhang, A. Erwin, Z. Zhang, A. P. Sokolov, J. Nanda and T. Saito, *ACS Energy Lett.*, **4**, 1171 (2019).
7. A. Miranda, K. Sarang, B. Gendensuren, E.-S. Oh, J. Lutkenhaus and R. Verduzco, *Mol. Syst. Des. Eng.*, **5**, 709 (2020).
8. J. Li, R. B. Lewis and J. R. Dahn, *Electrochem. Solid-State Lett.*, **10**, A17 (2007).
9. A. Magasinski, B. Zdyrko, I. Kovalenko, B. Hertzberg, R. Burtovyy, C. F. Huebner, T. F. Fuller, I. Luzinov and G. Yushin, *ACS Appl. Mater. Interfaces*, **2**, 3004 (2010).
10. H.-K. Park, B.-S. Kong and E.-S. Oh, *Electrochem. Commun.*, **13**, 1051 (2011).
11. I. Kovalenko, B. Zdyrko, A. Magasinski, B. Hertzberg, Z. Milicev, R. Burtovyy, I. Luzinov and G. Yushin, *Science*, **334**, 75 (2011).
12. S.-L. Chou, J.-Z. Wang, H.-K. Liu and S.-X. Dou, *J. Phys. Chem. C*, **115**, 16220 (2011).
13. G. T. Kim, S. S. Jeong, M. Joost, E. Rocca, M. Winter, S. Passerini and A. Balducci, *J. Power Sources*, **196**, 2187 (2011).
14. M. Mancini, F. Nobili, R. Tossici, M. Wohlfahrt-Mehrens and R. Marassi, *J. Power Sources*, **196**, 9665 (2011).
15. S.-J. Kim, B.-R. Lee and E.-S. Oh, *J. Power Sources*, **273**, 608 (2015).
16. B.-R. Lee, S.-j. Kim and E.-S. Oh, *J. Electrochem. Soc.*, **161**, A2128 (2014).
17. S.-W. Han, S.-J. Kim and E.-S. Oh, *J. Electrochem. Soc.*, **161**, A587 (2014).
18. C. He, B. Gendensuren, H. Kim, H. Lee and E.-S. Oh, *J. Electroanal. Chem.*, **876**, 114532 (2020).
19. S. Lee, E.-Y. Kim, H. Lee and E.-S. Oh, *J. Power Sources*, **269**, 418 (2014).
20. L. Gong, M. H. T. Nguyen and E.-S. Oh, *Electrochem. Commun.*, **29**, 45 (2013).
21. M. H. T. Nguyen and E.-S. Oh, *Electrochem. Commun.*, **35**, 45 (2013).
22. A. Ragheb, I. A. Ei-Thalouth, M. A. Amer, S. H. Nassar and M. Kamel, *Starch - Stärke*, **45**, 244 (1993).
23. B. R. Sharma, V. Kumar and P. L. Soni, *Starch - Stärke*, **55**, 38 (2003).
24. G. Rajput, I. P. Pandey, G. Joshi and S. S. Bisht, *J. Indian Acad. Wood*

Sci., **12**, 1 (2015).
25. D. N. Iqbal, A. Nazir, M. Iqbal and M. Yameen, *Green Process. Synth*., **9**, 212 (2020).
26. J. He, J. Wang, H. Zhong, J. Ding and L. Zhang, *Electrochim. Acta*, **182**, 900 (2015).
27. V. Singh, A. Tiwari, D. N. Tripathi and R. Sanghi, *J. Appl. Polym. Sci*., **92**, 1569 (2004).
28. V. Singh, A. Tiwari, S. Pandey, S. K. Singh and R. Sanghi, *J. Appl. Polym. Sci*., **104**, 536 (2007).
29. L. Zhang, J.-D. Zhang and B.-J. Xu, *Results Phys*., **19**, 103583 (2020).
30. Y. Wang, Y. Zhang, W.-J. Yang, S. Jiang, X. Hou, R. Guo, W. Liu, P. Huang, J. Lu, H. Gu and J. Xie, *J. Electrochem. Soc*., **166**, A5014 (2018).
31. L. Mo and H. Zheng, *Energy Rep*., **6**, 2913 (2020).
32. Y.-H. Jin, K.-M. Min, H.-W. Shim, S.-D. Seo, I.-S. Hwang, K.-S. Park and D.-W. Kim, *Nanoscale Res. Lett*., **7**, 10 (2012).
33. M. Ratynski, B. Hamankiewiecz, M. Krajewski, M. Boczar, D. A. Buchberger and A. Czerwinski, *Electrocatalysis*, **11**, 160 (2020).
34. T. R. Jow, S. A. Delp, J. L. Allen, J.-P. Jones and M. C. Smart, *J. Electrochem. Soc*., **165**, A361 (2018).
35. Z. Ogumi, *Electrochemistry*, **78**, 319 (2010).
36. M. Opitz, J. Yue, J. Wallauer, B. Smarsly and B. Roling, *Electrochim. Acta*, **168**, 125 (2015).
37. B. Gendensuren and E.-S. Oh, *J. Power Sources*, **384**, 379 (2018).
38. T. Kim, W. Choi, H.-C. Shin, J.-Y. Choi, J. M. Kim, M.-S. Park and W.-S. Yoon, *J. Electrochem. Sci. Technol*., **11**, 14 (2020).
39. F. Croce, S. D. Brown, S. G. Greenbaum, S. M. Slane and M. Salomon, *Chem. Mater*., **5**(9), 1268 (1993).
40. Y.-S. Kim, Y.-G. Cho, D. Odkhuu, N. Park and H.-K. Song, *Sci. Rep*., **3**, 1917 (2013).
41. D. Zhou, Y.-B. He, R. Liu, M. Liu, H. Du, B. Li, Q. Cai, Q.-H. Yang and F. Kang, *Adv. Energy Mater*., **5**, 1500353 (2015).
42. S. Karuppiah, S. Franger and K. Nallathamby, *ChemElectroChem*., **5**, 343 (2018).
43. M. Yoo, C. W. Frank and S. Mori, *Chem. Mater*., **15**, 850 (2003).

Supporting Information

Cyanoethyl-guar gum as an effective polymer binder for lithium titanate electrode of the lithium-ion battery

Inyeong Choi[‡], Bolormaa Gendensuren[‡], Jieun Lee, and Eun-Suok Oh[†]

School of Chemical Engineering, University of Ulsan, 93 Daehakro, Nam-gu, Ulsan 44610, Korea
(*Received 21 July 2022 • Revised 31 October 2022 • Accepted 29 December 2022*)

Table S1. The electrode composition and the mass loading of the LTO electrodes in binder-related LTO papers published within last few years

Years	Title	DOI	Objective binder	Slurry content ratio AM : CM : Binder, wt%	Mass loading of AM, mg cm^{-2}
Present study	Cyanoethyl-Cuar Gum as a Effective Polymer Binder for Lithium Titanate Electrode of the Lithium-Ion battery (In this study)		Cyanoethyl-Guar Gum (CGG)	LTO : SP : binder 85 : 10 : 5 87 : 10 : 3 90 : 5 : 5	4.0-6.2±0.1
2017	Different Shades of $Li_4Ti_5O_{12}$ Composites: The Impact of the Binder on Interface Layer Formation	10.1002/celc.201700395	PAA-Na and CMC-Na	LTO : CB : binder 90 : 6 : 4	2.4-3.6
2018	Water-Soluble Green Binder for $Li_4Ti_5O_{12}$ Anodes: Effect of Binder Choice on Lithium Storage	10.1002/celc.201700963	LA132	LTO : CB : binder 70 : 20 : 10	3.2±0.01
2018	Water-processable $Li_4Ti_5O_{12}$ electrodes featuring eco-friendly sodium alginate binder	10.1016/j.electacta.2018.09.017	Sodium alginate (SA)	LTO : CB : binder 87 : 10 : 3 90 : 7 : 3	2.0-3.0
2019	Highly conductive NMP-free carbon-coated nano-lithium titanate/carbon composite electrodes via SBR-assisted electrophoretic deposition	10.1016/j.electacta.2018.12.166	SBR	LTO : AB : binder 80 : 10 : 10	6.4±0.5
2019	Investigation on polyvinyl alcohol and sodium alginate as aqueous binders for lithium-titanium oxide anode in lithium-ion batteries	10.1007/s11581-018-2751-8	PVA, Sodium alginate (SA)	LTO : SP : binder 85 : 10 : 5 88 : 10 : 2	4.8±0.2
2020	Electrochemical performance of polysaccharides modified by the introduction of SO_3H as binder for high-powered $Li_4Ti_5O_{12}$ anodes in lithium-ion batteries	10.1016/j.jelechem.2020.114532	Sylfonated polysaccharides as S-SA and S-CMC	LTO : SP : binder 80 : 10 : 10	3.0±0.5
2020	Enhancement of the lithium titanium oxide anode performance by the copolymerization of conductive polypyrrole with poly(acrylonitrile/butyl acrylate) binder	10.1007/s10800-020-01401-8	PANBA-Ppy	LTO : SP : CMC : binder 90 : 5 : 2 : 3	5.2±0.5
2020	Study on Different Water-Based Binders for $Li_4Ti_5O_{12}$ Electrodes	10.3390/molecules25102443	PVDF/SA and PVDF/CMC blend	LTO : CB : binder 90 : 6 : 4	

Table S1. Continued

Years	Title	DOI	Objective binder	Slurry content ratio AM : CM : Binder, wt%	Mass loading of AM, mg cm^{-2}
2020	Instability of PVDF Binder in the $LiFePO_4$ versus $Li_4Ti_5O_{12}$ Li-Ion Battery Cell	10.1002/hlca.202000183	PVDF	LTO: CM: binder 80:10:10	
2021	Rheological Properties of Aqueous Sodium Alginate Slurries for LTO Battery Electrodes	10.3390/polym13203582	Sodium alginate (SA) with vs. surfactant in slurry	LTO:SP:binder 90:6:4	
2021	Locust bean gum as green and water-soluble binder for $LiFePO_4$ and $Li_4Ti_5O_{12}$ electrodes	10.1007/s10800-020-01496-z	Locust bean gum (LBG)	LTO:CB:binder 85:5:10	2.0-3.0
2022	Deciphering the Interplay between Binders and Electrolytes on the Performance of $Li_4Ti_5O_{12}$ Electrodes for Li-Ion Batteries	10.3390/en15124182	Sodium alginate (SA)	LTO:CB: binder 90:7:3 87:10:3 80:10:10	2.0-5.0

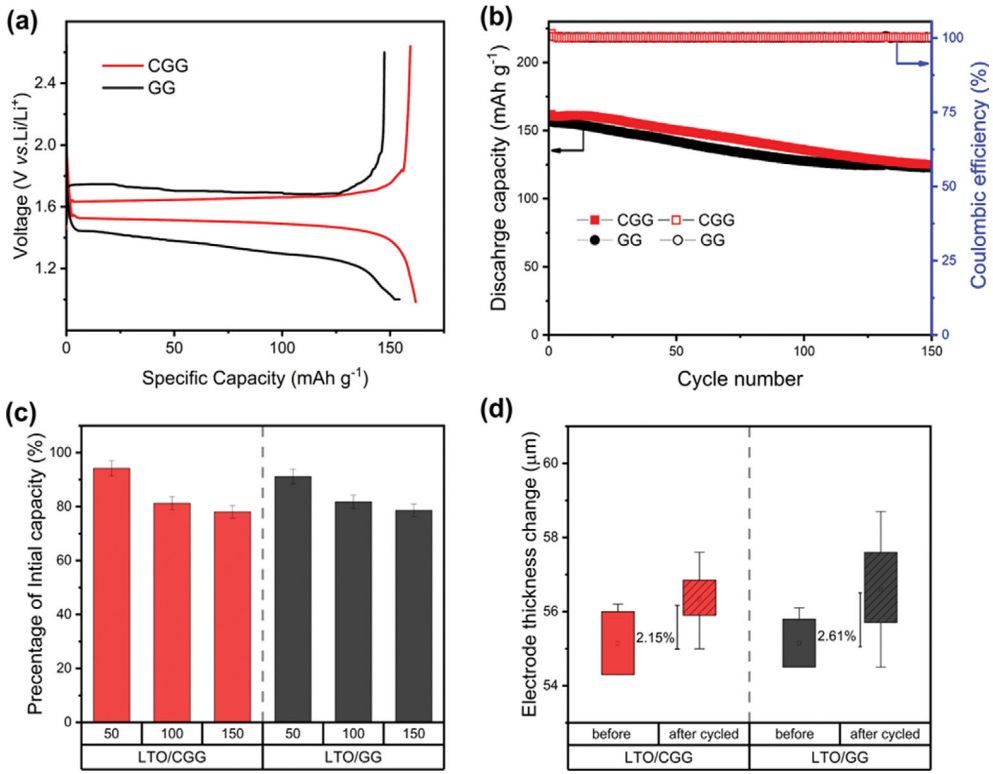

Fig. S1. The electrochemical performance of the high mass loading of the LTO electrodes: (a) Initial charge-discharge profiles at 0.1 C, (b) cycling performance at 1 C, (c) capacity fading of the LTO electrodes at 50th, 100th, and 150th cycles and, (d) the electrode thickness changes after 150 cycles.

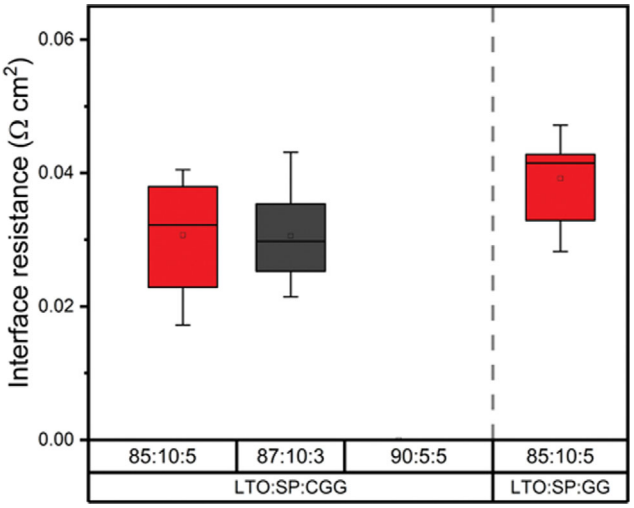

Fig. S2. The interface resistance between the electrode layer and the current collector of the LTO electrode sheets measured by a 46-probe system.

Table S2. Electrolyte uptake and ionic conductivities of GG and CGG binders

	GG	CGG
Electrolyte uptake for 2 days (%)	25.5	25.0
Ionic conductive ($\times 10^{-7}$ S cm^{-1})	1.87	2.59